ARTICLE

Functionalized Metal-organic Frameworks for White Light Emission and Highly Sensitive Sensing of PA and Fe^{3+}/Al^{3+}①

HUANG Jing-Jing ZHAO Dan YIN Guo-Jie②

(*Luoyang Institute of Science and Technology, Luoyang* 471023*, China*)

ABSTRACT Three isomorphic Ln-MOFs [Ln(bcbob)(H_2O)(DMF)] (Ln = Tb for **1**, Eu for **2**, Gd for **3**; DMF = *N*,*N*-dimethylformamide) have been constructed from a semi-rigid V-shaped organic linker 3,5-bis((4′-carboxylbenzyl)oxy)benzoilate acid (H_3bcbob) under solvothermal conditions. X-ray single-crystal diffraction analysis reveals that they exhibit a two-dimensional (2D) layered structure. Compounds **1**~**3** show the characteristic green and red emissions of Ln^{3+} and blue emission arising from the organic ligand, respectively. Based on their photoluminescence properties, the white-light emitting materials **4** and **5** with longer fluorescence lifetime (ms grade) and higher quantum yield (*e.g.* 40.61% for **4**) are fabricated. Remarkably, **1** exhibits good sensing ability on nitroaromatic compounds, especially for picric acid (PA). In addition, **1** is still a highly selective sensing material for Fe^{3+} and Al^{3+}.

Keywords: lanthanide organic frameworks, aromatic carboxylic acid, fluorescence, doping, chemical sensingdiiron; DOI: 10.14102/j.cnki.0254-5861.2011-3304

1 INTRODUCTION

In recent years, the government has been concerned about environmental matter such as water, air and industrial-waste pollution, etc. due to the hazards they pose to human health. To our knowledge, nitroaromatic compounds are widely utilized in industries for various chemical synthesis and explosive materials. But their notorious environmental pollution and explosiveness nature make them high dangerous to living things and human life. Among these explosives, picric acid (PA) has been generally used in the fields of medicines, explosives, paper making and textile. However, it is high toxic and may cause male infertility, anemia and other severe health problems[1, 2]. Meanwhile, iron plays a key role in the metabolic process for organisms. A shortage of iron element or an excess would also cause serious health problems to humans[3-5]. The traditional methods for pollution-detection require complicated instruments and are high-cost. Accordingly, it is extremely important and urgent to develop novel methods that are highly efficient and can be applied to a variety of pollutants.

Metal-organic frameworks (MOFs), as a very important class of multifunctional inorganic-organic hybrid materials, have received tremendous attention due to their structural diversity[6, 7], and the potential applications in gas storage and separation[8-12], fluorescent sensors[13-19], drug delivery[20-24] and catalysis[25-30]. Among diversity applications, the luminescent lanthanide-based MOFs (Ln-MOFs) play an important role in sensing and detecting due to their distinguishing advantages as large Stokes shifts, high luminescence efficiency, narrow emission peaks, high color purity and relative long fluorescent lifetime. However, the direct excitation of lanthanide luminescence materials was restrained by the forbidden 4*f*-4*f* transition. The luminescence performance of most Ln-MOFs is usually sensitized based on specific energy transfer from organic chromophores bearing π-conjugated centers to Ln^{3+} sites, which are known as "antenna effect"[31, 32]. In recent decades, aromatic carboxylate ligands have been broadly applied in the synthesis of Ln-MOFs, because they exhibit unique optical properties

Received 7 July 2021; accepted 24 January 2022

① Supported by the High-level Talents Initiation Project of Luoyang Institute of Technology (2018BZ17), the Pre-research Project of Luoyang Institute of Technology (2018YZ15), the Key Scientific Research Project of Higher Education of Henan Province (20B150016), the Training Program for Young Backbone Teachers of Higher Education of Henan Province (2020GGJS243) and the Science and Technology Project of Henan Province (182102210102, 202102210058)

② Corresponding author. E-mail: 13523612522@163.com

and interesting structural features.

Besides, Ln-MOFs offer a platform for the development of functional luminescent materials, in particular those with white-light emission. Considering that Ln-MOFs are usually isomorphic and the spatial regularity of their construction units in such structures provides the probability of incorporating distinct Ln^{3+} into one framework without damage to the original framework structures, these mixed Ln-MOFs can simultaneously generate the emission colors of different Ln^{3+}. And finally, white-light emission can be achieved by precise modulation of the relative amount of different Ln^{3+} and by varying the excitation wavelength[33-35].

As a semi-rigid V-shaped ligand, 3,5-bis((4′-carboxylbenzyl)oxy)benzoilate acid (H_3bcbob, Scheme 1) endowed with three carboxylic groups has diverse bridging modes to construct multi-dimensional MOFs. Previously, H_3bcbob, 1,2-bis(4-pyridyl)-ethene (bpe) and 1,2-bis(4-piperidyl)-propane (bpp) were used in our group to construct several fascinating frameworks. Herein, via utilizing H_3bcbob as a bridging ligand, three isomorphous Ln-MOFs [Ln(bcbob)(H_2O)(DMF)] (Ln = Tb for **1**, Eu for **2**, Gd for **3**) with a 2D layered structure are firstly prepared under solvothermal conditions. Based on their photoluminescence properties, we successfully fabricate two white-light emitting materials **4** and **5** by precise modulation of the relative amount of distinct Ln^{3+} and varying the rational excitation wavelength. Remarkably, **1** exhibits good sensing ability on nitroaromatic compound, especially for picric acid (PA). In addition, **1** is still a highly selective sensing material for Fe^{3+} and Al^{3+}.

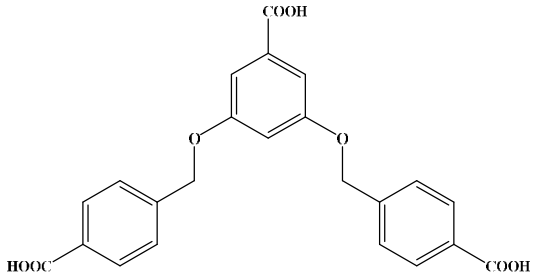

H_3bcbob

Scheme 1. Molecular structure of H_3bcbob

2 EXPERIMENTAL

2. 1 Common materials and general methods

The materials and solvents used were purchased from specific merchant, and further purification procedures were not performed. Infrared (IR) spectrum test was recorded on a Perkin Elmer Spectrum 1 spectrophotometer (4000~400 cm^{-1}) via utilizing a powder material on a KBr salver. Powder X-ray diffraction (PXRD) data were smoothly collected on a Rigaku/max-2550 diffractometer with Cu-$K\alpha$ radiation (λ = 1.5418 Å). Elemental analysis (C, H and N) was performed on a Pekin-Elmer 2400LS II elemental analyzer. Thermogravimetric (TG) behavior was investigated on a Pekin-Elmer TGA-7 instrument with a heating rate of 10 $^oC \cdot min^{-1}$ in air. Fluorescence spectra were recorded on a LS 55 fluorescence/phosphorescence spectrophotometer at 298 K. Commission International de l'Eclairage (CIE) color coordinates were calculated on the basis of international CIE standards. Fluorescence lifetime and quantum yield were measured on an Edinburgh Instrument FLS920 steady-state transient fluorescence spectrometer at 298 K.

2. 2 Synthesis of the title complex

[Tb(bcbob)(H_2O)(DMF)] 1 A mixture of $Tb(NO_3)_3 \cdot 6H_2O$ (23 mg, 0.05 mmol) with H_3bcbob (21 mg, 0.05 mmol) and DMF (6 mL) (acidified to pH = 4 by 6M HNO_3) was heated to 160 ^{o}C for 3 days, and subsequently cooled to room temperature. The obtained colorless columnar crystals were collected, washed with DMF, and dried in air. Yield: *ca.* 42% based on Tb(III). Anal. Calcd. for $C_{26}H_{24}NO_{10}Tb$ **1**: C, 46.65; H, 3.61; N, 2.09. Found: C, 46.69; H, 3.59; N, 2.66%. IR (cm^{-1}): 1660 (m), 1593 (s), 1539 (m), 1423 (s), 1375 (s), 1150 (s), 1051 (s), 864 (m), 836 (m), 784 (s), 715 (w), 673 (w), 640(w), 598 (w).

[Eu(bcbob)(H_2O)(DMF)] 2 The colorless crystals **2** in column were obtained from a similar self-assembly to that of **1** except $Eu(NO_3)_3 \cdot 6H_2O$ (22 mg, 0.05 mmol) in place of $Tb(NO_3)_3 \cdot 6H_2O$. Yield: *ca.* 40% based on Eu(III). Anal. Calcd. for $C_{26}H_{24}NO_{10}Eu$ **2**: C, 46.77; H, 3.62; N, 2.10. Found: C, 46.63; H, 3.67; N, 2.53%. IR (cm^{-1}): 1664 (m), 1589 (s), 1537 (m), 1419 (s), 1372 (s), 1148 (s), 1047 (s), 862 (m), 834 (m), 782 (s), 713 (w), 670 (w), 638(w), 595 (w).

[Gd(bcbob)(H_2O)(DMF)] 3 The colorless crystals of **3** in column were acquired from a similar synthetic strategy to that of **1** except $Gd(NO_3)_3 \cdot 6H_2O$ (22 mg, 0.05 mmol) in place of $Tb(NO_3)_3 \cdot 6H_2O$. Yield: *ca.* 36% based on Gd(III). Anal. Calcd. for $C_{26}H_{24}NO_{10}Gd$ **3**: C, 47.17; H, 3.65; N, 2.11. Found: C, 46.94; H, 3.48; N, 2.43%. IR (cm^{-1}): 1662 (m), 1591 (s), 1539 (m), 1420 (s), 1374 (s), 1149 (s), 1049 (s), 864 (m), 835 (m), 783 (s), 714 (w), 672 (w), 639 (w), 597 (w).

[$Tb_{0.2}Eu_{0.35}Gd_{0.45}$(bcbob)($H_2O$)(DMF)] 4 The colorless columnar single crystals **4** were gained from a similar building methods to that of **1** except $Tb(NO_3)_3 \cdot 6H_2O$,

$Eu(NO_3)_3·6H_2O$ and $Gd(NO_3)_3·6H_2O$ (0.05 mmol, molar ratio: 0.2:0.35:0.45) in place of $Tb(NO_3)_3·6H_2O$. Yield: *ca.* 35% based on H_3bcbob. IR (cm^{-1}): 1661 (w), 1595 (s), 1538 (w), 1418 (s), 1371 (m), 1301 (w), 1145 (s), 1047 (s), 864 (w), 835 (m), 783 (s), 716 (w), 669 (w), 635 (w), 597 (w).

$[Tb_{0.5}Eu_{0.5}$(bcbob)(H_2O)(DMF)] 5 The colorless crystals of **5** in column were acquired successfully from a similar construction methods to that of **1** except $Tb(NO_3)_3·6H_2O$ and $Eu(NO_3)_3·6H_2O$ (0.05 mmol, molar ratio: 0.5:0.5) in place of $Tb(NO_3)_3·6H_2O$. Yield: *ca.* 39% based on H_3bcbob. IR (cm^{-1}): 1666 (w), 1598 (s), 1540 (w), 1419 (s), 1372 (m), 1300 (w), 1146 (s), 1045 (s), 860 (w), 838 (m), 784 (s), 718 (w), 673 (w), 632 (w), 600 (w).

2. 3 X-ray structure determination

The powder X-ray single-crystal diffraction analysis reveals that **1-3** are isomorphic with each other. Compounds **2** and **3** have poor crystal quality and are unsuitable for single-crystal X-ray diffraction test. Table 1 provides the crystal data of complex **1**. The data were collected smoothly with Mo-$K\alpha$ radiation (λ = 0.71073 Å) on a Bruker APEX-II CCD diffractometer. Meanwhile, with the SHELXTL program, the structure of this complex was solved by direct methods[33]. In refinement, the non-hydrogen atoms were assigned anisotropic displacement parameters in the refinement. And the whole hydrogen atoms on the benzene rings were also treated rationally by using a riding model. In addition, the hydrogen atoms on the coordinated H_2O molecules were not located. The structure was then refined on F^2 using SHELXL-97[36]. The CCDC number is 1840267 for **1**. Crystal data for $C_{26}H_{24}NO_{10}Tb$ (M_r = 669.38 g/mol): monoclinic system, space group $C2/m$, a = 13.8958(6), b = 23.9513(11), c = 8.6270(9) Å, β = 103.164(1)°, V = 2795.8(3) $Å^3$, Z = 4, T = 273 K, μ(Mo-$K\alpha$) = 2.584 mm^{-1}, D_c = 1.590 g/cm^3, 35601 reflections measured ($5.4 \leqslant 2\theta \leqslant 55°$), 3288 unique ($R_{int}$ = 0.145, R_{sigma} = 0.0417) which were used in all calculations. The final R = 0.040 ($I > 2\sigma(I)$) and wR = 0.1103 (all data).

3 RESULTS AND DISCUSSION

3. 1 Structural description

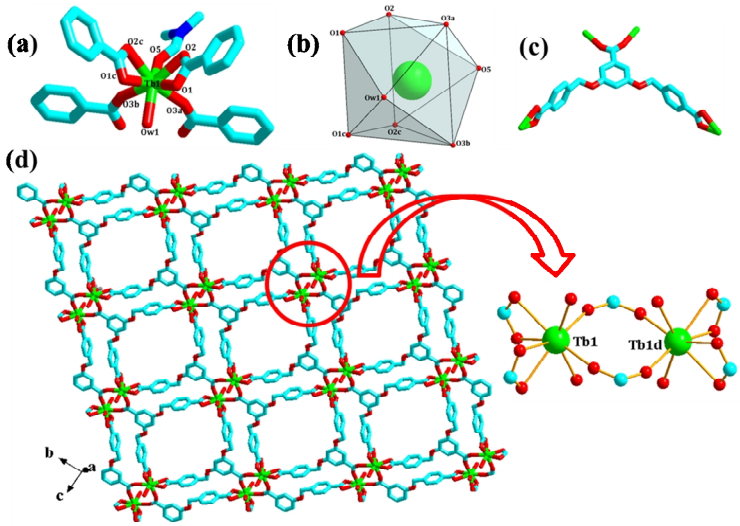

Fig. 1. Coordination environment around Tb1 (a), schematic representation of distorted TbO_8 distorted tricapped triangular prismatic coordination polyhedron (b), coordination modes of bcbob (c) and 2D network (only O atoms in DMF and H_2O are shown) in compound 1 (a: –*x*+1/2, –*y*+1/2, –*z*; b: –*x*+1/2, *y*–1/2, –*z*; c: *x*, –*y*, *z*; d: 1–*x*, *y*, 1–*z*)

X-ray single-crystal diffraction determination displays that **1** is a $bcbob^{3-}$-extended 2D Tb^{3+} coordination polymer. It crystallizes in space group $C2/m$, and the asymmetric unit is composed of a half Tb^{3+} ion, a half bcbob molecule, a half DMF molecule, and a half coordinated water molecule. As Fig. 1a shows, Tb1 with a distorted tricapped triangular prismatic geometry (Fig. 1b) is coordinated by six carboxylato O atoms (O(1), O(2), O(1c), O(2c), O(3a), O(3b)), one water molecule (O(w1)), and one DMF molecule (O(5)). The Tb1–O distances span a wide range from 2.287(8) to 2.484(9) Å. The $bcbob^{3-}$ ions connect four Tb^{3+} cations by acting as a hexadentate ligand through its three carboxyl groups based on two distinct coordination modes, μ_2-η^1:η^1 bis-monodentate bridging method and μ_1-η^1:η^1 chelating way (see Fig. 1c). Bridged by $bcbob^{3-}$, **1** self-assembles into a 2D layered network (Fig. 1d). The molecular stricter of **1** is basically planar,

and the three carboxylate groups are also coplanar with their corresponding aromatic rings, diverging in lateral directions. But, the carboxyphenyl rings at 3- and 5-positions are nearly perpendicular to the middle one (the dihedral angle between these planes is 86.2º). Two Tb^{3+} generate a dual-core building block, $Tb_2(COO)_6(H_2O)_2(DMF)_2$, with the Tb···Tb distance of 5.0366(17) Å. Then the adjacent binuclear units are bridged by flexible tripodal ligands, thus leading to a 2D network.

3. 2 Characterization

Fig. S1 presents the experimental and simulated powder XRD patterns of **1**~**5**. The experimental powder XRD pattern for **1**~**5** are in accord with the simulated one generated on the basis of structural data, confirming that the as-synthesized product is in pure phase and **1**~**5** are isomorphic.

The TG analyses of **1**~**3** were performed to investigate the thermal stability. As shown in Fig. S2, the curves indicate that three compounds have good thermal stability and exhibit similar thermal behavior due to their isomorphous nature. Hence, only **1** was taken as a representative example for discussion. Compound **1** underwent three steps of weight loss. A minor weight loss for the first step should be assigned to the removal of one coordinated water molecule (calcd.: 2.7%; found: 2.6%). The continuous weight loss in the temperature of 190~270 ºC corresponds to the loss of one DMF molecule (calcd.: 13.6%; found: 13.1%). In the third step, the organic molecule departed, and Tb^{3+} combined synchronously with O_2 into Tb_2O_3 (calcd.: 27.3%; found: 27.9%).

3. 3 Photoluminescence properties

The fluorescence properties of compounds **1**~**3** and H_3bcbob ligand were investigated in the solid state at 298 K. As shown in Fig. 2, once excited (λ_{ex} = 365 nm), the emission of H_3bcbob ligand exhibits a broad peak and with a maximum intensity at 425 nm maybe because of the bcbob-centered electronic transition ($\pi \rightarrow \pi^*$ or $n \rightarrow \pi^*$). Under excitation at 315 nm, **1** exhibits characteristic emission band of Tb^{3+} at 489, 545, 586 and 620 nm, corresponding to the $^5D_4 \rightarrow {}^7F_J$ (J = 6-3). And the hypersensitive peak at 544 nm determines the green-light emission of **1**. For the emission of **2** (λ_{ex} = 315 nm), the five peaks at 579, 591, 613, 652, and 699 nm should be assigned to the $^5D_0 \rightarrow {}^7F_J$ (J = 0–4) transition of the Eu^{3+} ion. The red light of **2** is dominated by the emission at 613 nm. Upon excitation at 360 nm, compound **3** exhibits a blue light emission with a wide band centered at 428 nm, which is quite similar to that of free H_3bcbob ligand, except for a slight red shift. Since the energy of the lowest excited states of Gd^{3+} $^6P_{7/2}$ is too high to accept the energy of the ligand, the characteristics emission peak of 4*f*-4*f* transition at 311 nm is not observable. Therefore, the emission peak of **3** at 433 nm should be attributed to the internal ligand $\pi^* \rightarrow \pi$ charge transfer.

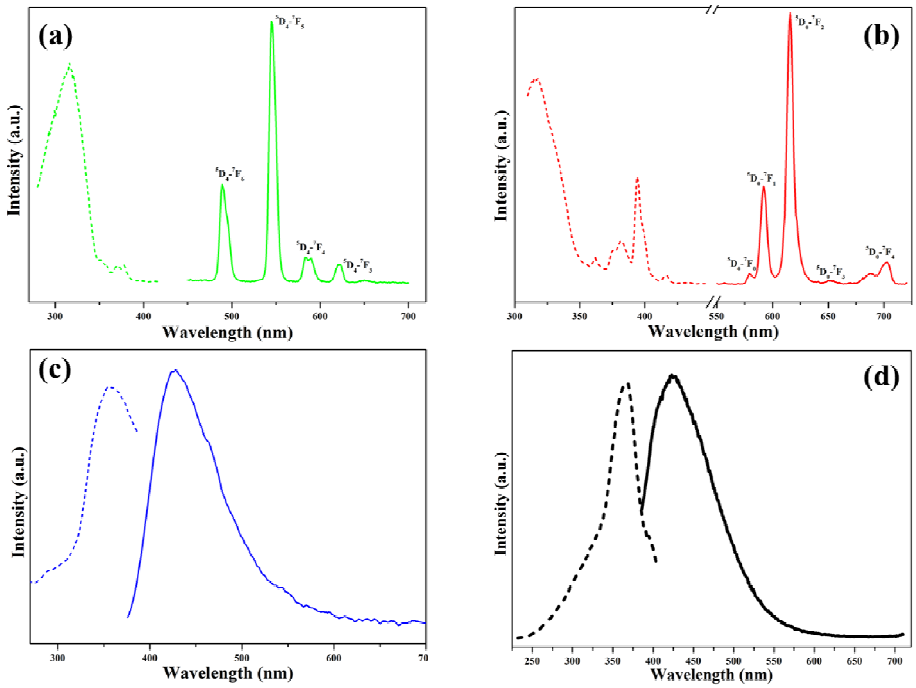

Fig. 2. Solid-state photoluminescence spectra of 1 (a), 2 (b), 3 (c) and H_3bcbob (d)

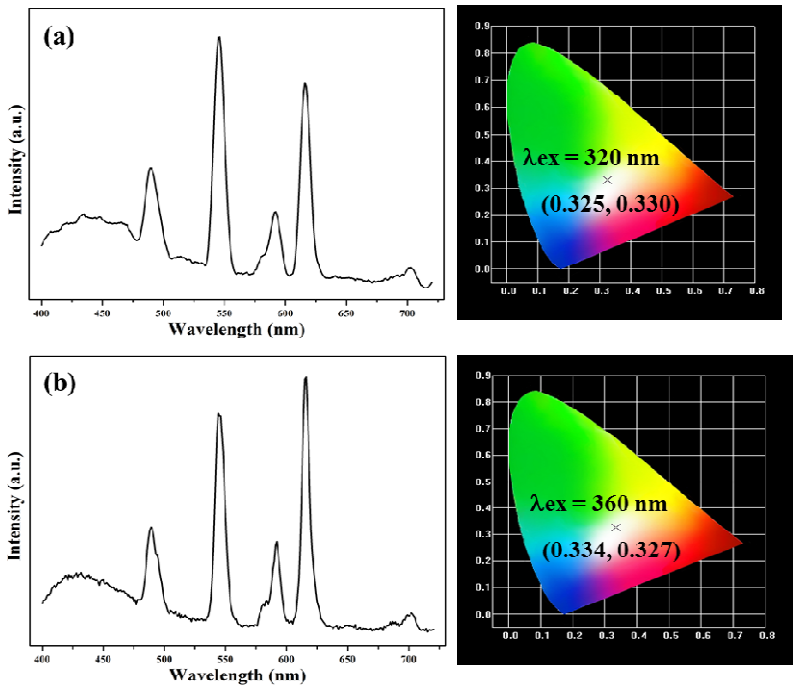

Fig. 3. Solid-state emission spectra and CIE chromaticity diagram for 4 (a) and 5 (b) excited at 360 nm

Compounds **1**~**3** emit RGB primary color, and they are isomorphic. Therefore, it is expected to obtain white-light photoluminescence by doping different Ln^{3+} into the identical framework. By precisely adjusting the ratio of $Tb^{3+}/Eu^{3+}/Gd^{3+}$, and finding suitable excitation wavelengths, white-light emitting compound **4** [$Tb_{0.2}Eu_{0.35}Gd_{0.45}$(bcbob)($H_2O$)-(DMF)] was successfully obtained. When excited at 320 nm, the corresponding CIE chromaticity coordinates (0.325, 0.330) are very close to those of the pure white light (0.333, 0.333), suggesting that **4** is a white-light emitting material (Fig. 3a). The quantum yield for **4** is 40.61%. Powder XRD analysis proves that **4** is isomorphic with **1**~**3** (Fig. S1).

Owing to its blue light emission, H_3bcbob ligand can be used as blue light sources, so the materials possessing white-light emitting characteristic might be acquired by doping Tb^{3+} and Eu^{3+} into one framework. When the conditions are appropriate, the combination of the "antenna effect" and the ligand luminescence can achieve white light emission. By carefully optimizing the molar ratio of Tb^{3+} and Eu^{3+}, we successfully designed and constructed white-light emitting compound **5** [$Tb_{0.5}Eu_{0.5}$(bcbob)(H_2O)(DMF)]. When excited at 360 nm, only part of the energy transfers from the ligand to the excited state of the Ln^{3+}. The remaining energy ensures itself to emit the blue light. The solid-state emission spectra and CIE chromaticity diagrams are shown in Fig. 3b. The corresponding CIE coordinate (0.334,0.327) at 360 nm is close to the coordinate for pure white light with the quantum yield to be13.46%. The Powder XRD analysis proves that **5** is isomorphic with **1**~**3** (Fig. S1).

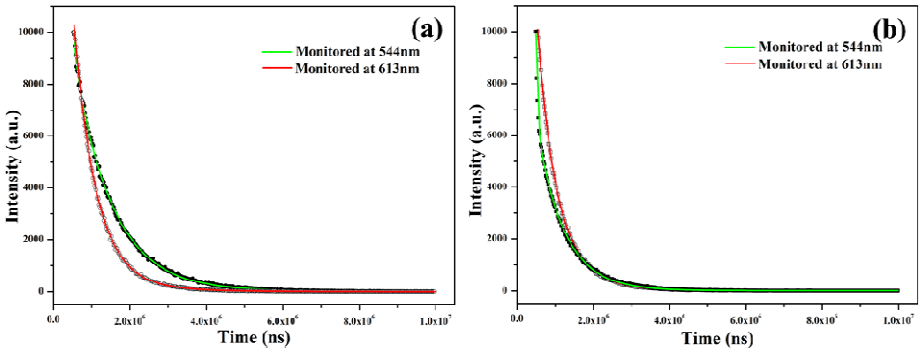

Fig. 4. Luminescence decay profiles of 4 (a) and 5 (b)

The efficient luminescence emission decay tests were executed for doped **4** and **5** at 298 K. And the decay curves are well fitted into a double exponential function: $I = I_0 + A_1\exp(-t/\tau_1) + A_2\exp(-t/\tau_2)$, in which τ_1 and τ_2 are construed as the luminescence lifetimes. A summary about the detailed fitting results is displayed in Table S1. In Fig. 4, the PL decay curves of **4** and **5** are recorded at 298 K accompanied by the emission monitored by the $^5D_4 \rightarrow {}^7F_5$ transition at 544 nm and the $^5D_0 \rightarrow {}^7F_2$ transition at 613 nm (λ_{ex} = 320 nm for **4** and λ_{ex} = 360 nm for **5**).

3. 4 Detection of nitro aromatics

Based on the photoluminescence properties of **1**, nitroaromatic compounds such as nitrobenzene (NB), 4-nitrotolune (4-NT), 2,4-dinitrotolune (2,4-DNT), 2,4-dinitrophenol (2,4-DNP) and picric acid (PA) were used for investigating the sensing properties of compound **1**. Before measurements were executed carefully, stable suspension was prepared with the steps as follows: a ground powder sample of **1** (3 mg) was dispersed in DMF solution of different quencher (3 mL, 100 mM), and then treated by ultrasonication for 30 min. As shown in Fig. 5a, the fluorescence spectrum of each suspension is similar to the spectrum in pure DMF, except that the emission intensity shows different degree of reduction. The decreasing order of quenching effect is PA > 2,4-DNP > 2,4-DNT > NB > 4-NT. Especially for PA, the quenching efficiency is as high as 80% (Fig. 5b). This indicates that **1** can detect trace amounts of nitro pollutants. Compound **1** is stable in these nitro aromatics, which is confirmed by the XRD pattern (Fig. S3).

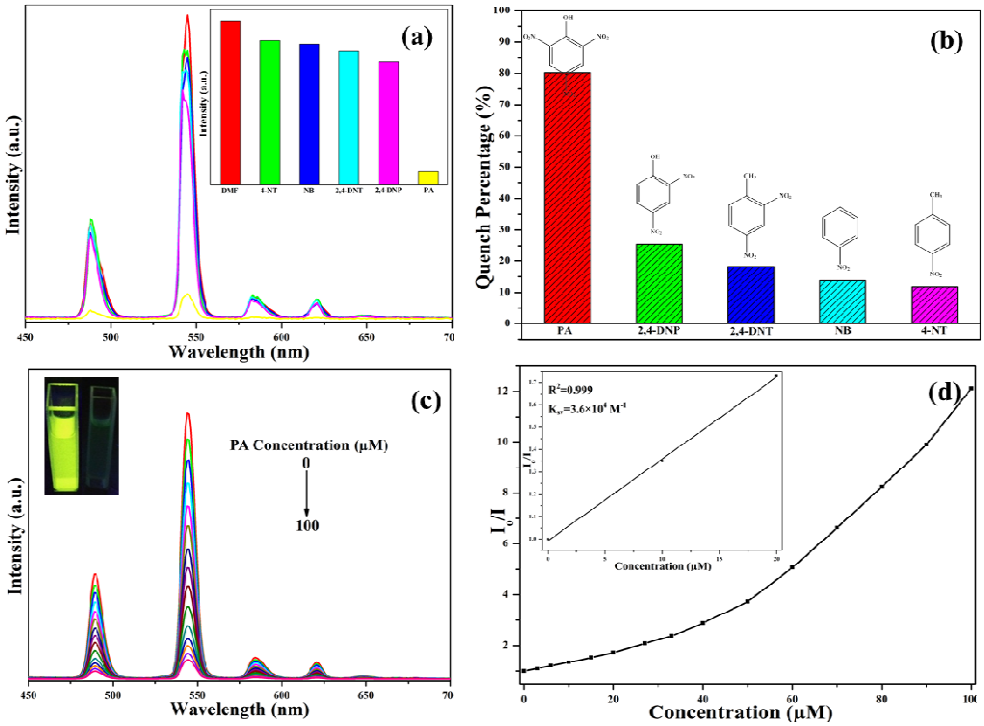

Fig. 5. Photoluminescence behaviors of 1 in the presence of nitroaromatic compounds with a concentration of 100 μM (a), photoluminescence quench percentage (b); Emission spectra of 1 with gradually increased PA (Inserted plot showing a fluorescence change after adding PA) (c), and Stern-Volmer plot of I_o/I *vs* the concentration of PA (Inserted plot being Stern-Volmer plot at lower concentrations)

To investigate in depth the quenching efficiency of the PA materials, the emission behaviors of suspensions of **1** with different PA concentration were measured. The powder **1** (3 mg) was dispersed into 3 mL DMF to generate a suspension. And then PA was gradually added into this suspension. With the increases of PA concentration, the fluorescence intensity of the suspension gradually decreases (Fig. 5c). When the PA concentration is 6 μM, the fluorescence intensity of **1** decreases by 19%, while the PA concentration is 100 μM, and the fluorescence intensity of **1** reduces by 92%. Fig. 5d gives the Stern-Volmer plot of relative fluorescence intensity (I_o/I) *vs* PA concentration, where I_o and I represent the fluorescence intensity of **1** before and after adding PA. The fitting curve at low concentration field is a good linear (R^2 = 0.999). The calculated K_{sv} value is 3.6 × 10^4 M^{-1}, which is equivalent to the data in the reported literature. The fluorescence

quenching caused by PA should be the process of the interaction between the electron donor and acceptor. H_3bcbob is an electron-rich ligand that can act as an electron donor. Nitro compounds are typical electron-deficient materials and are potential electron acceptors. When **1** contacts PA, the energy transfer path in **1** will change. The energy from H_3bcbob is transferred to PA, instead of being transferred to the Tb^{3+}. Namely, PA destroys the "antenna effect" of the ligand, resulting in fluorescence quenching. In addition, there is a π-conjugated structure in **1**, so a fluorescent signal can be rapidly given once encountering PA.

3. 5 Detection of metal ions

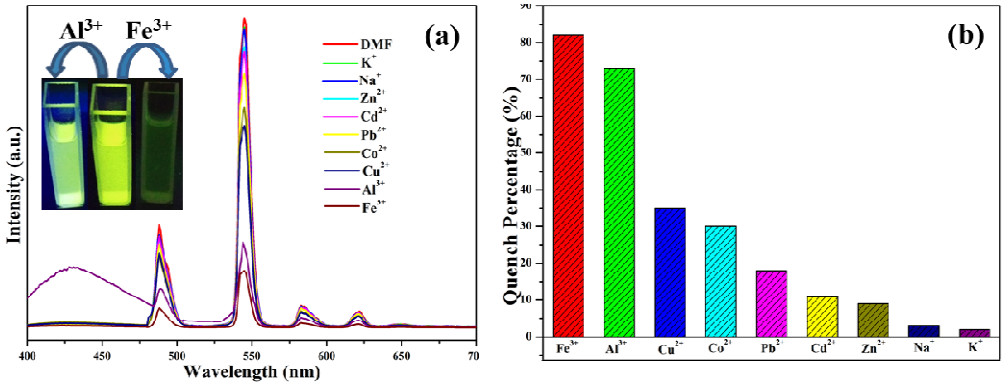

Fig. 6. Photoluminescence behaviors of 1 in various $M(NO_3)_x$ solutions with a concentration of 100 μM (Insert shows the fluorescence change after adding Fe^{3+} and Al^{3+} under the UV lamp (a), photoluminescence quench percentage (b))

In addition, we also investigate the sensing ability of **1** for various metal ions by the same method. The grounded powder samples (3 mg) were dispersed in DMF solutions (3 mL) with different metal ions, and the fluorescence intensity of each suspension was measured after 30 min of ultrasonication. As shown in Fig. 6, the fluorescence spectra show that various metal ions have different effects on the luminescence of **1**. When dispersed in different metal ions, the fluorescence intensity of **1** at 544 nm does not decrease significantly except Al^{3+} and Fe^{3+} solutions. However, the fluorescence spectra of **1** in Al^{3+} and Fe^{3+} solutions are obviously different. Fe^{3+} has a great quenching effect on luminescence intensity (quenching efficiency is 82%); Al^{3+} quenches the emission of Tb^{3+} and enhances the emission of the ligand, giving rise to a blue light. This suggests that **1** is has high selectivity for Fe^{3+} and Al^{3+}.

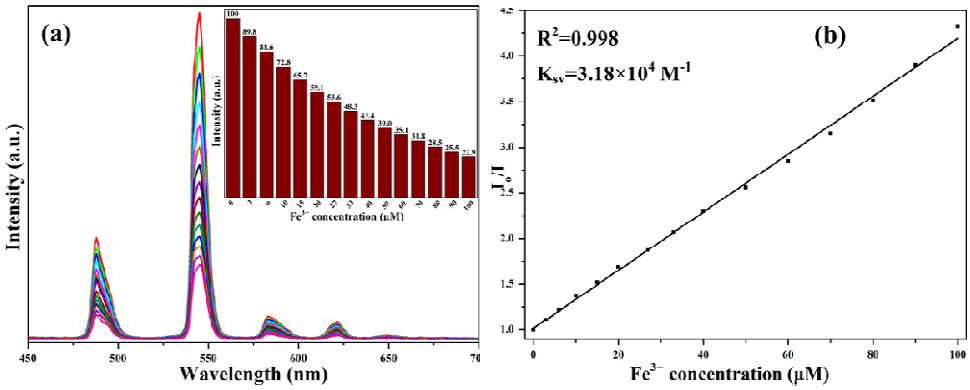

Fig. 7. Emission spectra of 1 with gradually increased Fe^{3+} (a) and Stern-Volmer plot of I_0/I *vs* concentration of Fe^{3+} (b)

In order to better understand the fluorescence response of **1** to Fe^{3+} and Al^{3+}, the fluorescence change of the suspension was measured with increasing the ion concentration. The powder samples were ground and immersed in different concentrations of Fe^{3+} or Al^{3+}, and then their luminescence spectra were recorded. As demonstrated in Fig. 7, with the increase of Fe^{3+} concentration, the emission intensity of suspension decreases gradually. Fig. 7b gives the fitting cure of the Stern-Volmer plot, which is in good agreement with the linear equation (R^2 = 0.998). The calculated K_{sv} value is 3.18×10^4 M^{-1}, which is equivalent to the data reported[37-39]. As shown in Fig. 8a, with the increase of Al^{3+} concentration,

the luminescence intensity of **1** at 544 nm gradually decreases and the emission of the ligand gradually increases. When the concentration is 100 mM, the luminescence of Tb^{3+} is nearly completely quenched and only the emission of the ligand can be observed. In order to observe this process more directly, we take pictures of the suspension with corresponding concentration under UV light irradiation at 365 nm, finding that the suspension changes from green to bright blue (Fig. 8b). Simultaneously, we discover that the framework of **1** dissolves gradually with increasing the Al^{3+} concentration. When the Al^{3+} concentration reaches 0.1 mM, the solution is completely clear. According to the previous literatures, the quenching effect on luminescence MOFs by metal ions may be attributed to the following factors: i) interactions between metal ions and organic ligands[40-41]; 2) destruction of the crystal structure by the metal ions[42]; 3) ion exchange between the central metal ions of the framework and the targeted cations[43-44]. The powder XRD patterns of **1** in different metal ion solutions disclosed that Fe^{3+} did not destroy the framework of the compound (Fig. S4). We speculate that the fluorescence quenching caused by Fe^{3+} should be the interaction between and the O atom in the structure. The fluorescence quenching caused by Al^{3+} should be the collapse of the framework of **1**.

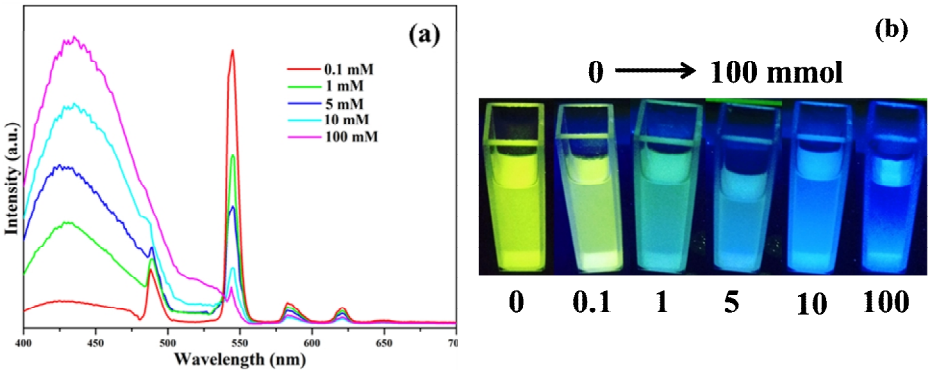

Fig. 8. Emission spectra of 1 in the presence of different concentration of Al^{3+} (a) and the corresponding photographs for 1 in the presence of different concentrations of Al^{3+} under UV-light (b)

4 CONCLUSION

In summary, using flexible ligand 3,5-bis((4′-carboxylbenzyl)oxy)benzoilate acid (H_3bcbob) as linker, three 2D isomorphic Ln-MOFs **1-3** have been constructed under solvothermal conditions. Based on their photoluminescence properties, two white-light emitting materials **4** and **5** were fabricated. Compounds **4** and **5** possess longer fluorescence lifetime and higher quantum yields, which should be due to the larger π-conjugated structure of $bcbob^{3-}$. Systematical fluorescence quenching studies show that **1** can highly sensitively sense the different nitroaromatic compounds, especially for PA (K_{sv} = 3.6 ´ 10^4 M^{-1}). The fluorescence quenching of **1** should be related to the electron deficient nature for PA. Due to their electron deficient nature, the intrinsic energy transferring path is changed and the “antenna effect” is prohibited, so the quenching phenomenon occurs. In addition, **1** is a highly selectively sensing material for Fe^{3+} (K_{sv} = 3.18 ´ 10^4 M^{-1}) and Al^{3+} (enhance the ligand luminescence).

REFERENCES

(1) Hu, Z.; Deibert, B. J.; Li J. Luminescent metal-organic frameworks for chemical sensing and explosive detection. *Chem. Soc. Rev.* **2014**, 43, 5815–5840.

(2) Song, X. Z.; Song, S. Y.; Zhao, S. N.; Hao, Z. M.; Zhu, M.; Meng, X.; Wu, L. L.; Zhang, H. J. Single-crystal-to-single-crystal transformation of a europium(III) metal-organic framework producing a multi-responsive luminescent sensor. *Adv. Funct. Mater.* **2014**, 24, 4034−4041.

(3) Arici, M. Luminescent 2D + 2D → 2D interpenetrated Zn(II)-coordination polymer based on reduced Schiff base tricarboxylic acid and bis(imidazole) ligand for detection of picric acid and Fe^{3+} ions. *Cryst. Growth Des.* **2017**, 17, 5499–5505.

(4) Ju, Z.; Yan, W.; Gao, X.; Shi, Z.; Wang, T.; Zheng, H. Syntheses, characterization, and luminescence properties of four metal-organic frameworks based on a linear-shaped rigid pyridine ligand. *Cryst. Growth Des.* **2016**, 16, 2496–2503.

(5) Tian, D.; Li, Y.; Chen, R. Y.; Chang, Z.; Wang, G. Y.; Bu, X. H. A luminescent metal-organic framework demonstrating ideal detection ability for

nitroaromatic explosives. *J. Mater. Chem. A* **2014**, 2, 1465–1470.

(6) Dang, L.; Li, T. T.; Cui, Z.; Sui, D.; Ma, L. F.; Jin, G. X. Selective construction and stability studies of a molecular trefoil knot and Solomon link. *Dalton Trans.* **2021**, 50, 16984–16989.

(7) Dang, L.; Li, T. T.; Zhao, C. C.; Zhang, T. T.; Ye, X. Y.; Sun, X. T.; Wang, H. R.; Ma, L. F. Supramolecular Rh6 catalytic system promoting directed [4+4] cycloaddition reaction of anthracene under UV irradiation. *J Solid State Chem.* **2022**, 306, 122785–122792.

(8) Hilal, D.; Hasan, C. G.; Gokay, A.; Gokhan, O. A.; Omer, F. A.; Cigdem, A.; Ilknur, E.; Seda, K. Effect of metal-organic framework (MOF) database selection on the assessment of gas storage and separation potentials of MOFs. *Angew. Chem. Int. Ed.* **2021**, 60, 7828–7837.

(9) Rogacka, J.; Seremak, A.; Luna-Triguero, A.; Formalik, F.; Matito-Martos, I.; Firlej, L.; Calero, S.; Kuchta, B. High-throughput screening of metal-organic frameworks for CO_2 and CH_4 separation in the presence of water. *Chem. Eng. J.* **2021**, 403, 126392–126402.

(10) Daglar, H.; Keskin, S. Recent advances, opportunities, and challenges in high-throughput computational screening of MOFs for gas separations. *Coord. Chem. Rev.* **2020**, 422, 213470–213490.

(11) Fan, W.; Wang, X.; Xu, B.; Wang, Y.; Liu, D.; Zhang, M.; Shang, Y.; Dai, F.; Zhang, L.; Sun D. Amino-functionalized MOFs with high physicochemical stability for efficient gas storage/separation, dye adsorption and catalytic performance. *J. Mater. Chem. A* **2018**, 6, 24486–24495.

(12) Erucar, I.; Keskin, S. Unlocking the effect of H_2O on CO_2 separation performance of promising MOFs using atomically detailed simulations. *Ind. Eng. Chem. Res.* **2020**, 59, 3134–3152.

(13) Sushil, K.; Siddhant, S.; Arun, K.; Pramod, K. Recognition, mechanistic investigation and applications for the detection of biorelevant $Cu^{2+}/Fe^{2+}/Fe^{3+}$ ions by ruthenium(II)-polypyridyl based fluorescent sensors. *Dalton Trans.* **2021**, 50, 2705–2721.

(14) Wu, S.; Min, H.; Shi, W.; Cheng, P. Multicenter metal-organic framework-based ratiometric fluorescent sensors. *Adv. Mater.* **2019**, 1805871.

(15) Jin, J.; Xue, J.; Liu, Y.; Yang, G.; Wang, Y. Recent progresses in luminescent metal-organic frameworks (LMOFs) as sensors for the detection of anions and cations in aqueous solution. *Dalton Trans.* **2021**, 50, 1950–1972.

(16) Yang, M. Q.; Zhou, C. P.; Chen, Y.; Li, J. J.; Zeng, C. H.; Zhong, S. Highly sensitive and selective sensing of CH_3Hg^+ via oscillation effect in Eu-cluster. *Sens. Actuators B* **2017**, 248, 589−596.

(17) Li, Y.; Li, S.; Yan, P.; Wang, X.; Yao, X.; An, G.; Li, G. Luminescence-colour-changing sensing of Mn^{2+} and Ag^+ ions based on a white-light-emitting lanthanide coordination polymer. *Chem. Commun.* **2017**, 53, 5067–5070.

(18) Wu, S.; Lin, Y.; Liu, J.; Shi, W.; Yang, G.; Cheng, P. Rapid detection of the biomarkers for carcinoid tumors by a water stable luminescent lanthanide metal-organic framework sensor. *Adv. Funct. Mater.* **2018**, 1707169.

(19) Sun, Z.; Sun, J.; Xi, L.; Xie, J.; Wang, X.; Ma, Y.; Li, L. Two novel lanthanide metal-organic frameworks: selective luminescent sensing for nitrobenzene, Cu^{2+}, and MnO_4^-. *Cryst. Growth Des.* **2020**, 20, 5225–5234.

(20) Protap, B.; Parthasarathi, D. Anchoring drugs to a zinc(II) coordination polymer network: exploiting structural rationale toward the design of metallogels for drug-delivery applications. *Inorg. Chem.* **2021**, 60, 3218–3231.

(21) Sun, X.; He, G.; Xiong, C.; Wang, C.; Lian, X.; Hu, L.; Li, Z. One-pot fabrication of hollow porphyrinic MOF nanoparticles with ultrahigh drug loading toward controlled delivery and synergistic cancer therapy. *ACS Appl. Mater. Interfaces* **2021**, 13, 3679–3693.

(22) Liu, X.; Liang, T.; Zhang, R.; Ding, Q.; Wu, S.; Li, C.; Lin, Y. Iron-based metal-organic frameworks in drug delivery and biomedicine. *ACS Appl. Mater. Interfaces* **2021**, 13, 9643–9655.

(23) Lawson, H. D.; Walton, S. P.; Chan, C. Metal-organic frameworks for drug delivery: a design perspective. *ACS Appl. Mater. Interfaces* **2021**, 13, 7004–7020.

(24) Wang, L.; Zheng, M.; Xie, Z. Nanoscale metal-organic frameworks for drug delivery: a conventional platform with new promise. *J. Mater. Chem. B* **2018**, 6, 707–717.

(25) Guo, T.; Mo, K.; Zhang, N.; Xiao, L.; Liu, W.; Wen, L. Embedded homogeneous ultra-fine Pd nanoparticles within MOF ultra-thin nanosheets for heterogeneous catalysis. *Dalton Trans.* **2021**, 50, 1774–1779.

(26) Das, A.; Anbu, N.; Mostakim, S. K.; Dhakshinamoorthy, A.; Biswas, S. A functionalized UiO-66 MOF for turn-on fluorescence sensing of superoxide in water and efficient catalysis for Knoevenagel condensation. *Dalton Trans.* **2019**, 48, 17371–17380.

(27) Zhang, L.; Yuan, S.; Fan, W.; Pang, J.; Li, F.; Guo, B.; Zhang, P.; Sun, D.; Zhou, H. Cooperative sieving and functionalization of Zr metal-organic frameworks through insertion and post-modification of auxiliary linkers. *ACS Appl. Mater. Interfaces* **2019**, 11, 22390–22397.

(28) Hou, S.; Dong, J.; Zhao, B. Formation of C–X bonds in CO_2 chemical fixation catalyzed by metal-organic frameworks. *Adv. Mater.* **2020**, 32,

1806163.

(29) Lu, B.; Yang, J.; Liu, Y.; Ma, J. A polyoxovanadate-resorcinarene-based porous metal-organic framework as an efficient multifunctional catalyst for the cycloaddition of CO_2 with epoxides and the selective oxidation of sulfides. *Inorg. Chem.* **2017**, 56, 11710–11720.

(30) Li, T. T.; Dang, L. L.; Zhao, C. C.; Lv, Z. Y.; Yang, X. G.; Zhao, Y.; Zhang, S. H. A self-sensitized Co(II)-MOF for efficient visible-light-driven hydrogen evolution without additional cocatalysts. *J. Solid State Chem.* **2021**, 304, 122609–122614.

(31) Xu, L.; Wang, Z.; Wang, R.; Wang, L.; He, X.; Jiang, H.; Tang, H.; Cao, D.; Tang, Z. A conjugated polymeric supramolecular network with aggregation-induced emission enhancement: an efficient light-harvesting system with an ultrahigh antenna effective. *Angew. Chem. Int. Ed.* **2020**, 59, 9908–9913.

(32) Sun, Z.; Hu, P.; Ma, Y.; Li, L. Lanthanide organic frameworks for luminescence sensing of nitrobenzene and nitrophenol with high selectivity. *Dyes Pigm.* **2017**, 143, 10–17.

(33) Liu, J.; Sun, W.; Liu, Z. White-light emitting materials with tunable luminescence based on steady Eu(III) doping of Tb(III) metal-organic frameworks. *RSC Adv.* **2016**, 6, 25689–25694.

(34) Yang, Y.; Chen, L.; Jiang, F.; Yu, M.; Wan, X.; Zhang, B.; Hong, M. A family of doped lanthanide metal-organic frameworks for wide-range temperature sensing and tunable white light emission. *J. Mater. Chem. C* **2017**, 5, 1981–1989.

(35) Huang, J. J.; Yu, J. H.; Bai, F. Q.; Xu, J. Q. White-light-emitting materials and highly sensitive detection of Fe^{3+} and polychlorinated benzenes based on Ln-metal-organic frameworks. *Cryst. Growth Des.* **2018**, 18, 5353–5364.

(36) Sheldrick, G. M. A. Short history of Shelx. *Acta Crystallogr., Sect. A: Found. Crystallogr.* **2008**, 64, 112–122.

(37) Zhong, F.; Zhang, X.; Zheng, C.; Xu, H.; Gao, J.; Xu, S. A fluorescent titanium-based metal-organic framework sensor for nitroaromatics and nanomolar Fe^{3+} detection. *J. Solid State Chem.* **2020**, 288, 121391–121397.

(38) Wang, X. Q.; Tang, J.; Ma, X.; Wu, D.; Yang, J. A water-stable zinc(II)-organic framework as an "on-off-on" fluorescent sensor for detection of Fe^{3+} and reduced glutathione. *CrystEngComm* **2021**, 23, 1243–1250.

(39) Zhang, J.; Ren, S.; Xia, H.; Jia, W.; Zhang, C. AIE-ligand-based luminescent Cd(II)-organic framework as the first "turn-on" Fe^{3+} sensor in aqueous medium. *J. Mater. Chem. C* **2020**, 8, 1427–1432.

(40) Tang, Q.; Liu, S.; Liu, Y.; Miao, J.; Li, S.; Zhang, L.; Shi, Z.; Zheng, Z. Cation sensing by a luminescent metal-organic framework with multiple lewis basic sites. *Inorg. Chem.* **2013**, 52, 2799–2801.

(41) Chen, B.; Wang, L.; Xiao, Y.; Fronczek, F. R.; Xue, M.; Cui, Y.; Qian, G. A Luminescent metal-organic framework with Lewis basic pyridyl sites for the sensing of metal ions. *Angew. Chem. Int. Ed.* **2009**, 48, 500–503.

(42) Cao, L. H.; Shi, F.; Zhang, W. M.; Zang, S. Q.; Mak, T. C. Selective sensing of Fe^{3+} and Al^{3+} ions and detection of 2,4,6-trinitrophenol by a water-stable terbium-based metal-organic framework. *Chem. Eur. J.* **2015**, 21, 15705–15712.

(43) Dang, S.; Ma, E.; Sun, Z. M.; Zhang, H. A layer-structured Eu-MOF as a highly selective fluorescent probe for Fe^{3+} detection through a cation-exchange approach. *J. Mater. Chem.* **2012**, 22, 16920–16926.

(44) Zhou, Y.; Chen, H. H.; Yan B. An Eu^{3+} post-functionalized nanosized metal-organic framework for cation exchange-based Fe^{3+}-sensing in an aqueous environment. *J. Mater. Chem. A* **2014**, 2, 13691–13697.